THE JOURNAL OF PHYSICAL CHEMISTRY B

Article

pubs.acs.org/JPCB

Mixed Quantum-Classical Molecular Dynamics Study of the Hydroxyl Stretch in Methanol/Carbon-Tetrachloride Mixtures II: Excited State Hydrogen Bonding Structure and Dynamics, Infrared Emission Spectrum, and Excited State Lifetime

Kijeong Kwac* and Eitan Geva*

Department of Chemistry, University of Michigan, Ann Arbor, Michigan 48109-1055, United States

ABSTRACT: We present a mixed quantum-classical molecular dynamics study of the hydrogen-bonding structure and dynamics of a vibrationally excited hydroxyl stretch in methanol/carbon-tetrachloride mixtures. The adiabatic Hamiltonian of the quantum-mechanical hydroxyl is diagonalized on-the-fly to obtain the ground and first-excited adiabatic energy levels and wave functions which depend parametrically on the instantaneous configuration of the classical degrees of freedom. The dynamics of the classical degrees of freedom are determined by Hellmann−Feynman forces obtained by taking the expectation value of the force with respect to the ground or excited vibrational wave functions. Polarizable force fields are used which were previously shown to reproduce the experimental infrared absorption spectrum rather well, for different isotopomers and over a wide composition range [Kwac, K.; Geva, E. *J. Phys. Chem. B* **2011**, *115*, 9184]. We show that the agreement of the absorption spectra with experiment can be further improved by accounting for the dependence of the dipole moment derivatives on the configuration of the classical degrees of freedom. We find that the propensity of a methanol molecule to form hydrogen bonds increases upon photoexcitation of its hydroxyl stretch, thereby leading to a sizable red-shift of the corresponding emission spectrum relative to the absorption spectrum. Treating the relaxation from the first excited to the ground state as a nonadiabatic process, and calculating its rate within the framework of Fermi's golden rule and the harmonic-Schofield quantum correction factor, we were able to predict a lifetime which is of the same order of magnitude as the experimental value. The experimental dependence of the lifetime on the transition frequency is also reproduced. Nonlinear mapping relations between the hydroxyl transition frequency and bond length in the excited state and the electric field along the hydroxyl bond axis are established. These mapping relations make it possible to reduce the computational cost of the mixed quantum-classical treatment to that of a fully classical treatment.

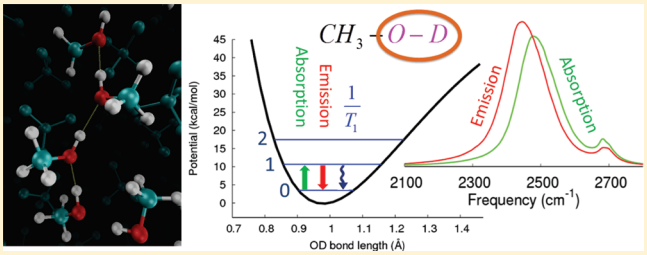

I. INTRODUCTION

The ability of alcohols to form hydrogen (H) bonds and the fact that they are amphiphilic and therefore highly miscible in nonpolar liquids over an extremely wide range of compositions make nonaqueous mixtures of alcohols with nonpolar liquids into attractive model systems for studying H-bonding. Strong evidence from both experimental and computational studies suggests that alcohols form H-bonded oligomers in such mixtures and that the distribution in size and structure of these oligomers depends on the composition.[1−13] The fact that H-bonds break and form on the picosecond time scale also leads one to expect these oligomers to exhibit complex dynamical behavior.[5,8,11,12,14−35]

The fact that the transition frequency of the hydroxyl stretch in alcohol oligomers is very sensitive to its H-bonding environment has made infrared (IR) spectroscopy of the hydroxyl stretch into a powerful probe of H-bonding in these systems.[14,15,20−30] More specifically, distinctly different spectral features can be assigned to contributions from the monomers (α) and hydroxyls that serve as H-bond acceptors (β), donors (γ), simultaneous acceptors and donors (δ) and simultaneous double-acceptors and donors (ε).[13] Generally speaking, the spectral features associated with the different hydroxyl subpopulations red shift and broaden with increasing participation of the hydroxyl in H-bonding. The relatively rapid rate of H-bond breaking and forming also implies that the transition frequencies of individual hydroxyls fluctuate both between and within those bands on the picosecond time scale.[22−30,36]

Another quantity that has been shown to be sensitive to H-bonding is the hydroxyl stretch excited state lifetime.[37] More specifically, recent two-color pump−probe measurements have shown that the lifetime of the hydroxyl stretch in methanol/CCl_4 mixtures decreased from 9 ps for the monomer to 0.45 ps for a strongly H-bonded methanol.[38,39] Hydroxyl lifetime measurements in ethanol/CCl_4 mixtures revealed a similar

Received: December 7, 2011
Revised: January 24, 2012
Published: January 30, 2012

   dx.doi.org/10.1021/jp211792j | *J. Phys. Chem. B* 2012, 116, 2856−2866

trend of decreasing lifetime with decreasing transition frequency, which correlates with increasing participation in H-bonding (from 0.9 ps at 3451 cm^{-1} to 0.25 ps at 3330 cm^{-1}).[40] More recent measurements of the lifetime of δ hydroxyls in 10 mol % mixtures of methanol-d (MeOD) in CCl_4 also revealed that the lifetime increased from 0.42 to 0.90 ps as the frequency increased from 2450 to 2550 cm^{-1}.[24] In contrast, the lifetime of β MeOD has been reported to be 2.15 ps.[22,23]

While molecular dynamics (MD) simulations are often employed nowadays for obtaining a molecular level understanding of structural and dynamical trends in complex condensed phase systems, quantitative MD-based modeling of IR spectra remains a rather formidable challenge. This is particularly true in the case of high-frequency modes, such as the hydroxyl stretch, in highly structured solutions, such as mixtures of alcohols with nonpolar liquids. In a recent paper[13] we have demonstrated how, by combining mixed quantum-classical methodology with the appropriate choice of force fields, one can obtain a model which is consistent with the experimental absorption IR spectrum of the hydroxyl stretch in methanol/CCl_4 mixtures, for different isotopomers and over a wide range of compositions. In order to achieve this level of consistency without adjustable parameters, we found that one has to account for the anharmonic nature of the hydroxyl stretch and polarizable nature of the force fields, as well as the damping of the polarizability at short distances. We have also shown that it is possible to establish nonlinear mapping relations between the hydroxyl transition frequency and bond length at the ground state and the electric field along the hydroxyl bond axis, which can be used to reduce the computational cost of the mixed quantum-classical treatment to that of a purely classical MD simulation.

In the present paper we show how the agreement of the absorption spectrum with experiment can be further improved by accounting for the explicit dependence of the dipole moment derivative on the classical degrees of freedom (DOF). We then extend the mixed-quantum-classical approach presented in ref 13 to the first excited state and use it in order to:

1. Explore how vibrational excitation affects the ability of the excited methanol molecule to form H-bonds with methanol molecules in its vicinity.
2. Estimate the spectral signature of the difference in H-bonding between the ground and excited states as reflected by the Stokes shift between the emission and absorption spectra of the hydroxyl stretch.
3. Test the ability of the force fields used for reproducing the experimental absorption spectrum to also reproduce the experimental excited state lifetime, as well as its dependence on the transition frequency.
4. Establish mapping relations between the hydroxyl transition frequency and bond length and the electric field along the hydroxyl bond axis that are appropriate for the excited state and test their ability to reduce the cost of computing the emission spectrum to that of a purely classical MD simulation.

The remainder of the paper is organized as follows. In section II, we outline the mixed quantum-classical approach, force-fields and methodology used for calculating absorption/emission spectra and vibrational lifetimes. In section III, we present results pertaining to the effect of accounting for the dependence of the dipole moment derivatives on the classical DOF, excited state H-bonding structure and dynamics, absorption/emission IR spectra, mapping relations and the excited state lifetimes. Summary and concluding remarks are provided in section IV.

II. THEORY AND SIMULATION TECHNIQUES

A. Mixed Quantum-Classical Molecular Dynamics. The mixed quantum-classical method employed here is the same as that described in ref 13 and will therefore only be briefly outlined. We consider a methanol/CCl_4 mixture where one of the hydroxyls, referred to as the tagged hydroxyl, is treated quantum-mechanically, while the remaining untagged DOF, referred to as the bath, are treated classically. For a given configuration of the bath DOF, $\mathbf{Q}$, we define the vibrational energy levels and corresponding stationary wave functions of the hydroxyl stretch as the eigenvalues and eigenfunctions of the adiabatic Hamiltonian

$$H_{ad}(\hat{q}, \hat{p}; \mathbf{Q})\Psi_n(q, \mathbf{Q}) = E_n(\mathbf{Q})\Psi_n(q, \mathbf{Q}) \tag{1}$$

where

$$H_{ad}(\hat{q}, \hat{p}; \mathbf{Q}) = K_q(\hat{p}) + V(\hat{q}, \mathbf{Q}) \tag{2}$$

Here n = 0, 1, 2, ... corresponds to the ground, first-excited, second-excited, etc. vibrational states of the tagged hydroxyl stretch, $K_q(\hat{p})$ is the vibrational kinetic energy of the tagged hydroxyl and $V(\hat{q},\mathbf{Q})$ is the overall potential energy.

In practice, the overall instantaneous configuration of the liquid solution is given in terms of the collection of the Cartesian coordinates of all atoms in the simulation cell, including the hydrogen associated with the tagged hydroxyl stretch

$$\begin{aligned}\mathbf{R} &= \{\mathbf{X}, \mathbf{Y}, \mathbf{Z}\}\\ &\equiv \{\mathbf{R}_k\}\\ &\equiv \{X_0, Y_0, Z_0, X_1, Y_1, Z_1, X_2, Y_2, Z_2, ..., X_N, Y_N, Z_N\}\end{aligned} \tag{3}$$

Here $\mathbf{R}_0 = (X_0,Y_0,Z_0)$ denotes the coordinates of the hydrogen associated with the tagged hydroxyl and $\{\mathbf{R}_k = (X_k,Y_k,Z_k)\}$ (k = 1,...,N) is the coordinates of all the remaining atoms, including the hydrogen atoms associated with the untagged hydroxyl stretches. The corresponding atomic momenta are given by

$$\mathbf{P} \equiv \mathbf{M}\cdot\dot{\mathbf{R}} \equiv \{M_0\dot{\mathbf{R}}_0...M_N\dot{\mathbf{R}}_N\} \tag{4}$$

where $\mathbf{M}\equiv(M_0,...,M_N)$ are the atomic masses. The total potential energy can then be written as

$$\begin{aligned}V(\mathbf{R}) = {} & V_1(X_0, Y_0, Z_0, ..., X_N, Y_N, Z_N)\\ & + U(X_1, Y_1, Z_1, ..., X_N, Y_N, Z_N)\end{aligned} \tag{5}$$

where V_1 represents the interaction between the tagged hydrogen and the remaining atoms and U represents all the interactions between the untagged atoms.

Within the mixed quantum-classical treatment, the Hellman–Feynman force on each of the atoms in the simulation box is explicitly dependent on the quantum state of the tagged hydroxyl stretch. Thus, when the tagged hydroxyl stretch is in

the nth quantum state, the force on the kth bath atom is given by

$$\mathbf{F}_k = -\nabla_k U - \int \mathrm{d}q\, |\Psi_n(q)|^2 \nabla_k V_1 \tag{6}$$

where $\nabla_k = (\partial/\partial X_k, \partial/\partial Y_k, \partial/\partial Z_k)$ and $k = 0, ..., N$. We also assume that the center of mass of the overall system is stationary so that the total force vanishes

$$\sum_{k=0}^{N} \mathbf{F}_k = 0 \tag{7}$$

Importantly, for a given overall configuration, $\mathbf{R}$, the value of q is uniquely determined, whereas knowledge of the adiabatic Hamiltonian, $\hat{H}_{\mathrm{ad}}(\hat{q},\hat{p};\mathbf{Q})$, requires knowledge of the explicit dependence of the potential energy on q for a given $\mathbf{Q}$ (see eq 2). In order to obtain the latter from the former, we evaluate the potential energy along a 41 point 1D grid of q values in the range 0.46 Å $\leq q \leq$ 1.46 Å by modifying $\mathbf{R}_0$ in such a way that only q changes while the remaining coordinates, including the bending angle and the dihedral angles associated with the tagged hydroxyl, are constrained at their original values. It should also be noted that after $\hat{H}_{\mathrm{ad}}(\hat{q},\hat{p};\mathbf{Q})$ is diagonalized, the values of $\mathbf{R}_0$ are reset so as to be consistent with the expectation value of $\hat{q}$ with respect to the new stationary state, $\overline{q} = \langle\Psi_n|\hat{q}|\Psi_n\rangle$. More details regarding the simulation algorithm can be found in ref 13. All the simulations reported in this paper were carried out using the AMBER 10 program package,[41] where the source code has been modified in order to implement the mixed quantum-classical algorithm outlined above.

B. Force Fields and Simulation Techniques. The vibrational dynamics of the tagged hydroxyl stretch is described by a Morse potential of the form

$$V_{\mathrm{vib}}(q) = D_0[1 - \mathrm{e}^{-a(q-q_0)}]^2 \tag{8}$$

where the values of the parameters are the same as in ref 13 (q_0 = 0.96131 Å, D_0 = 105.0 kcal/mol, a = 2.40414 Å^{-1}). The remaining untagged hydroxyl stretches are treated as harmonic using the standard AMBER force field parameters (i.e., spring constant of K_r = 553 kcal/(mol Å^2) and equilibrium length of r_{eq} = 0.96 Å). The remaining contributions to the potential energy are given by

$$\begin{aligned} V = &\sum_{\text{bonds}} K_r(r - r_{\mathrm{eq}})^2 + \sum_{\text{angle}} K_\theta(\theta - \theta_{\mathrm{eq}})^2 \\ &+ \sum_{\text{dihedral}} \frac{V_n}{2}[1 + \cos(n\varphi - \gamma)] \\ &+ \sum_{i<j} 4\varepsilon_{ij}\left[\left(\frac{\sigma_{ij}}{R_{ij}}\right)^{12} - \left(\frac{\sigma_{ij}}{R_{ij}}\right)^{6}\right] + \sum_{i<j} \frac{q_i q_j}{\varepsilon R_{ij}} + E_{\mathrm{pol}} \end{aligned} \tag{9}$$

Here K_r, K_θ, and V_n are force constants for bonds, angles, and dihedral terms; r_{eq} and θ_{eq} are equilibrium values for bond lengths and angles; n is the dihedral multiplicity; γ is the dihedral angle phase; ε_{ij} and σ_{ij} are Lennard-Jones potential parameters for ith and jth atoms; q_i is the charge of the ith atom; ε is the permittivity; and E_{pol} is the potential energy due to polarization (see ref 13 for more details). The force field parameters for methanol were adopted from the AMBER force field[41] and those for CCl_4 were adopted from ref 42. The polarizabilities, α, were adopted from ref 43. When polarizable force fields are used, the AMBER partial charges of methanol are multiplied by a scale factor of 0.88 as recommended by Caldwell and Kollman.[44]

Assigning specific constant values of the polarizability to each atom can result in unreasonably large induced dipole moments at sufficiently small interatomic distances. While this usually does not pose a problem in classical MD simulations,[45] this is not the case for mixed quantum-classical simulations. As pointed out in ref 13, this is because quantum delocalization of the tagged hydrogen allows it access to classically forbidden regions where it comes to be in close proximity with neighboring atoms. To this end, we modified the dipole−dipole interaction tensor according to the prescription proposed in refs 46−49 (see ref 13 for more details).

Most of the results reported in this paper were obtained from simulations carried out at 300 K on a 10 mol % mixture with 26 CH_3OD (MeOD) and 230 CCl_4 molecules within a cubic box whose size is adjusted so that the density is the same as the experimental value (6.5396×10^{-3} Å^{-3}). We also report some results for a 26 mol % mixture, which consist of 67 MeOD and 189 CCl_4 molecules in the simulation cell (density: 7.2345×10^{-3} Å^{-3}), and pure MeOD, with 256 MeOD molecules in the simulation cell (density: 15.4440×10^{-3} Å^{-3}). In each case, the system was equilibrated for 200 ps at 300 K using the fully classical Langevin dynamics with the collision frequency of 1.0 ps^{-1}. Following this, 400 configurations were sampled every 2 ps and used as initial configurations for the mixed quantum-classical MD runs. For each initial configuration thus obtained, we first randomized the initial velocities of the system by assigning velocities from Maxwell distribution at 300 K, followed by a 200 ps long Langevin dynamics trajectory at 300 K with the collision frequency of 1.0 ps^{-1}. This was then followed by a 35 ps mixed quantum-classical MD equilibration trajectory at the same temperature using the weak-coupling algorithm of Berendsen et al.,[50] which was then followed by a 50 ps mixed quantum-classical constant energy production run. The results reported below were obtained by averaging over 400 such production runs except the excited state lifetime, which is obtained by averaging over 10 000 classical MD runs with the nonlinear mapping relation and the procedure in section III.D.

In the analysis of H-bond structure and dynamics, the following criteria were used to define an H-bond: (1) O···D distance is less than 2.65 Å and (2) O···D−O angle is greater than 120° ("···" denotes H-bond).

C. IR Absorption and Emission Spectra. Within the mixed quantum-classical treatment, the IR absorption and emission spectra are calculated based on the following formula:[51]

$$I_k(\omega) = Re \int_0^\infty \mathrm{d}t\, J_k(t) \exp(i\omega t) \tag{10}$$

where k = 0 or 1 for absorption or emission, respectively, and

$$J_k(t) = \mathrm{e}^{-t/2T_1}\langle \mu_{01}(t)\mu_{10}(0) \exp[-i\int_0^t \mathrm{d}\tau\, \omega_{10}(\tau)]\rangle_k \tag{11}$$

Here,

$$\langle\cdots\rangle_k = \int \mathrm{d}\mathbf{Q}_0 \int \mathrm{d}\mathbf{P}_0 \frac{\exp[-\beta H_k(\mathbf{Q}_0, \mathbf{P}_0)}{Z_k}\cdots \tag{12}$$

dx.doi.org/10.1021/jp211792j | J. Phys. Chem. B 2012, 116, 2856−2866

where $H_k(\mathbf{Q}_0,\mathbf{P}_0) = K_B(\mathbf{P}_0) + E_k(\mathbf{Q}_0)$ and $Z_k = \int d\mathbf{Q}_0 \int d\mathbf{P}_0 \times \exp[-\beta H_k(\mathbf{Q}_0,\mathbf{P}_0)]$ are the classical bath Hamiltonian and partition function when the tagged hydroxyl is in the k-th vibrational state; $(\mathbf{Q}_0,\mathbf{P}_0)$ represents the initial coordinates and momenta of the bath DOF; $\mu_{ij}(t) = \langle\Psi_i(\mathbf{Q}_t)|\hat{\mu}|\Psi_j(\mathbf{Q}_t)\rangle$ is the transition dipole moment ($\hat{\mu}$ is the dipole moment operator, see section II.D for a more detailed discussion), $\omega_{10}(t) = [E_1(\mathbf{Q}_t) - E_0(\mathbf{Q}_t)]/h$ is the transition frequency and $\mathbf{Q}_t$ represents the coordinates of the bath DOF at time t as obtained via the classical dynamics on the adiabatic surface that corresponds to either the ground ($k = 0$) or first-excited ($k = 1$) vibrational states of the hydroxyl stretch. T_1 is the lifetime of the first-excited state, which is given by $T_1 = 0.5$ ps (see section II.E).

D. Transition Dipole Moments. In this paper, the transition dipole moments are calculated following a procedure which is somewhat different than that used in ref 13. We start out by expanding the dipole moment operator to first order in q around $q = q_0$

$$\mu = \mu_0 + \left.\frac{\partial\mu}{\partial q}\right|_{q=q_0} q \equiv \mu_0 + \mu' q \tag{13}$$

so that the transition dipole moment can be recast as

$$\mu_{ij}(t) = \mu'\langle\Psi_i(\mathbf{Q}_t)|\hat{q}|\Psi_j(\mathbf{Q}_t)\rangle \tag{14}$$

In ref 13 we assumed that μ' is a constant, so that only the dependence of the factor $\langle\Psi_i(\mathbf{Q}_t)|\hat{q}|\Psi_j(\mathbf{Q}_t)\rangle$ on the classical DOF was taken into account. In the present paper we also account for the dependence of μ' on the classical DOF. To this end, we follow a procedure similar to that used by Corcelli and Skinner in ref 52 in the case of water. More specifically, we used QM/MM in order to calculate μ' for 100 randomly chosen configurations taken from equilibrium ground state mixed quantum-classical MD simulations. The QM/MM calculation was based on the ONIOM method[53] as implemented in the Gaussian 09 package[54] and included all the molecules in the simulation box. Periodic boundary conditions were used in order to ensure that the tagged methanol is located at the center of the simulation box. The tagged methanol was then treated quantum-mechanically via DFT at the B3LYP/6-311+G(d,p) level, while the remaining molecules were treated classically using the nonpolarizable Amber force field. Geometry optimization was performed by constraining the coordinates of all DOF except the OD stretch, followed by a normal-mode analysis to calculate the vibrational frequency of the OD stretch and the corresponding dipole derivative.

In Figure 1 we show a correlation plot between μ' and the electric field along the hydroxyl stretch obtained for a 10 mol % MeOD in CCl_4. The value of μ' is seen to increase with the field by a factor of ~2 across the electric field range experienced by the hydroxyl. Furthermore, the correlation between μ' and the electric field can be treated as linear (the line in Figure 1 correspond to a linear least-squares fit). The fitting relation is $\mu' = 5.00004 + 114.778E$, where μ' is in Debye Å^{-1} amu$^{-1/2}$ and the electric field E in e/a_0^2.

Taking into account the linear mapping of μ' as a function of the electric field along the OD stretch, Figure 1, we recalculated the IR absorption spectrum of the hydroxyl in 10 mol % MeOD/CCl_4. The resulting calculated absorption spectrum is shown in Figure 2 alongside the experimental spectrum and the previously calculated absorption spectrum, where the variations

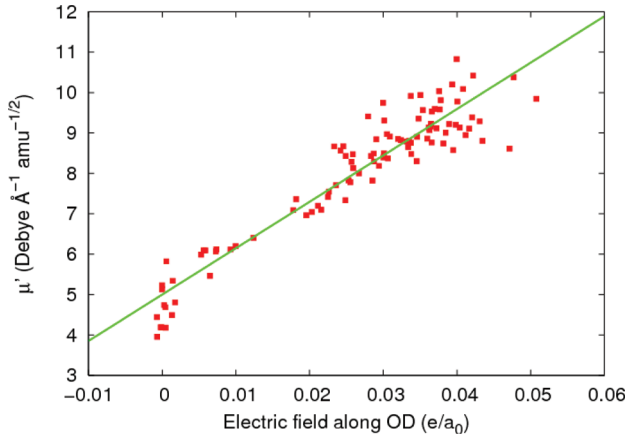

Figure 1. Correlation plot between μ' and the electric field along the hydroxyl stretch for 10 mol % MeOD/CCl_4 mixture. The line was obtained by a linear least-squares best fit.

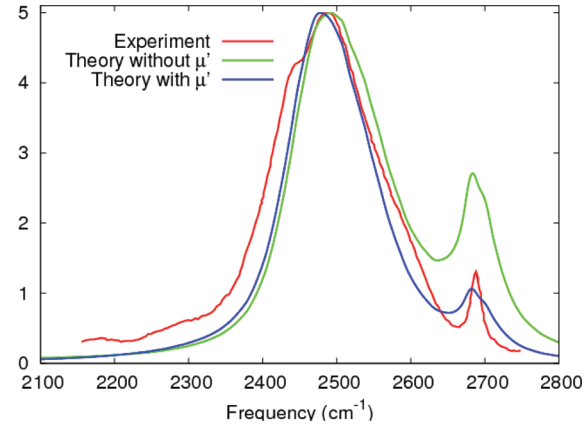

Figure 2. IR absorption spectrum of the hydroxyl in 10 mol % MeOD/CCl_4 mixture, calculated with (blue) and without (green) accounting for variations in the value of μ'. Also shown is the experimental absorption spectrum (red).

in the value of μ' were not accounted for.[13] As can be seen, accounting for the variation on μ' considerably improves the agreement between the calculated spectrum and the experimental one, particularly in the region of the high frequency $\alpha\beta$ band. As further evidence for the importance of accounting for the variation of μ', we have also recalculated the concentration dependence of the proportion of the $\alpha\beta$ band for CD_3OH in CCl_4. The resulting dependence is shown in Figure 3, alongside the experimental result and the previous result obtained without accounting for the variations in the value of μ'.[13] Here too, one observes the level of agreement with experiment to improve considerably when one accounts for the variation of μ'.

Skinner and co-workers have previously reported a similar correlation between μ' and the electric field in the case of HOD in H_2O or D_2O.[52,63] Those authors observed that the value of μ' in this system increases by a factor of 5 for across the relevant range of fields, as compared to the factor of 2 we observed for methanol. This observation is consistent with the view that H-bonding in water is stronger than in methanol.

E. Excited State Lifetime. The lifetime of the first-excited state of the hydroxyl stretch is obtained by treating the nonradiative relaxation process from the first excited to the

dx.doi.org/10.1021/jp211792j | J. Phys. Chem. B 2012, 116, 2856−2866

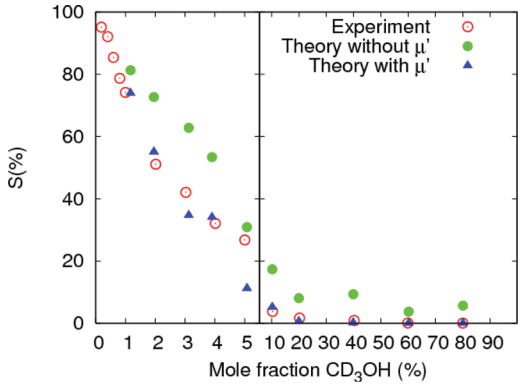

Figure 3. Proportion of areas of α/β band in the calculated IR absorption spectra of the OH stretch for ten different CD_3OH/CCl_4 mixtures in a concentration range between 1.17 and 80.08 mol %. Shown are results obtained with (blue) and without (green) accounting for variations in the values of μ'. Also shown are the experimental results (red) from ref 21.

ground state as a nonadiabatic transition within the framework of Fermi's golden rule

$$k_{01}(\langle\omega_{10}\rangle_1) \equiv \frac{1}{T_1} = Q_{HS}(\langle\omega_{10}\rangle_1)\int_{-\infty}^{\infty} dt\, \exp(i\langle\omega_{10}\rangle_1 t) \langle \exp(i\int_0^t d\tau\, \delta\omega_{10}(\mathbf{R}_\tau))[\mathbf{d}_{10}(\mathbf{R}_0)\cdot\dot{\mathbf{R}}_0][\mathbf{d}_{10}(\mathbf{R}_t)\cdot\dot{\mathbf{R}}_t]\rangle_1 \quad (15)$$

Here $T_1 = k_{01}^{-1}$ is the excited state lifetime, $\langle\omega_{10}(\mathbf{R})\rangle_1$ is the average emission frequency, $\delta\omega_{10}(\mathbf{R}_\tau) = \omega_{10}(\mathbf{R}_\tau) - \langle\omega_{10}\rangle_1$ is the deviation of the instantaneous transition frequency from the average value,

$$\mathbf{d}_{10}(\mathbf{R}) = \langle\psi_1(\mathbf{R})|\nabla_{\mathbf{R}}|\psi_0(\mathbf{R})\rangle \equiv -\frac{\langle\psi_1(\mathbf{R})|\nabla_{\mathbf{R}} V_1|\psi_0(\mathbf{R})\rangle}{\hbar\omega_{10}(\mathbf{R})} \quad (16)$$

is the nonadiabatic coupling vector,[55] and

$$Q_{HS}(\omega) = [e^{\beta\hbar\omega/2}\beta\hbar\omega/(1 - e^{-\beta\hbar\omega})]^{1/2} \quad (17)$$

is the harmonic-Schofield quantum correction factor.[56−58] The latter provide a simple way of accounting for the quantum nature of the bath spectral density at the relatively high frequency $\langle\omega_{10}(\mathbf{R})\rangle_1$.[57] We chose this quantum correction factor based on the suggestion in the work of Skinner and co-workers on the HOD−D_2O system.[65] It should be noted that more rigorous ways of accounting for the quantum nature of the bath, such as the linearized semiclassical method, are available.[59] However, the utilization of these methods for the system under study here will be reserved for a future study in light of its prohibitive computational cost.

III. RESULTS AND DISCUSSION

A. Radial Distribution Functions and Potentials of Mean-Force. In this section we employ various measures of molecular structure in order to establish that a vibrationally excited methanol molecule has a higher propensity for forming H-bonds in comparison to a methanol molecule in the ground vibrational state.

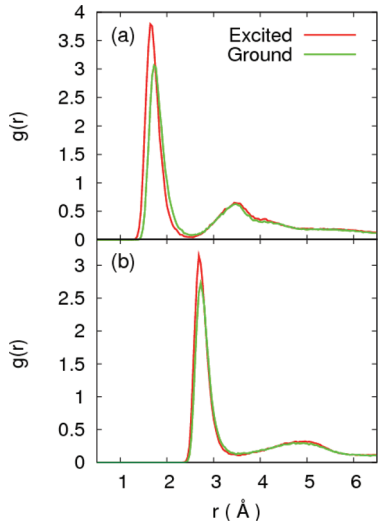

Figure 4. O−D (a) and O−O (b) radial distribution functions involving the D or O of the tagged OD stretch and the O of a neighboring MeOD, as obtained from a mixed quantum-classical MD simulation for the 10 mol % MeOD in CCl_4, when the tagged OD stretch is in the ground state (green) or first-excited state (red).

Figure 4 shows the D−O (a) and O−O (b) radial distribution functions (RDFs) involving the D or O of the tagged OD stretch and the O of a neighboring methanol molecule, as obtained from a mixed quantum-classical MD simulation of a 10 mol % MeOD/CCl_4 mixture, when the tagged OD stretch is either in the ground state (green) or first-excited state (red). The fact that the first peak of the D-O RDF in the excited state (height 3.9 and positioned at r = 1.655 Å) is larger and positioned at shorter distance than that in the ground state (height 3.1 and positioned at r = 1.735 Å) is consistent with a higher propensity for forming H-bonds in the excited state (see Figure 4a).

A similar trend is also observed for the O−O RDFs (see Figure 4b), where the first peak in the excited state (height 3.1 and positioned at r = 2.685 Å) is larger and positioned at a shorter distance than that in the ground state (height 2.8 and positioned at r = 2.715 Å). Yet another indication for the higher propensity for H-bonding in the excited state is the larger average OD bond length in the excited state (1.022 Å) in comparison to the ground state (0.989 Å).

Figure 5a shows the potential of mean force (PMF) as a function of the distance between the oxygen of the tagged OD stretch and the oxygen of the nearest-neighbor untagged methanol molecule, in the ground state (green) and in the first-excited state (red). The PMF is defined by $W(r) = -(k_BT)^{-1} \ln P(r)$ where $P(r)$ is probability density of the O−O distance. As expected, the excited-state PMF is shifted to shorter distances relative to the ground-state PMF.

Figure 5b shows the distribution of the O−D···O angle made by the tagged OD stretch and the oxygen of its nearest neighbor methanol, in the ground state (green) and first-excited state (red). The larger probability for angles greater than 160° in the excited state also suggests a higher propensity for H-bonding in the excited state.

B. Transition Frequency Distributions and Spectra. In this section, we examine the spectral signature on H-bonding, and particularly of the higher propensity of a vibrationally

dx.doi.org/10.1021/jp211792j | J. Phys. Chem. B 2012, 116, 2856−2866

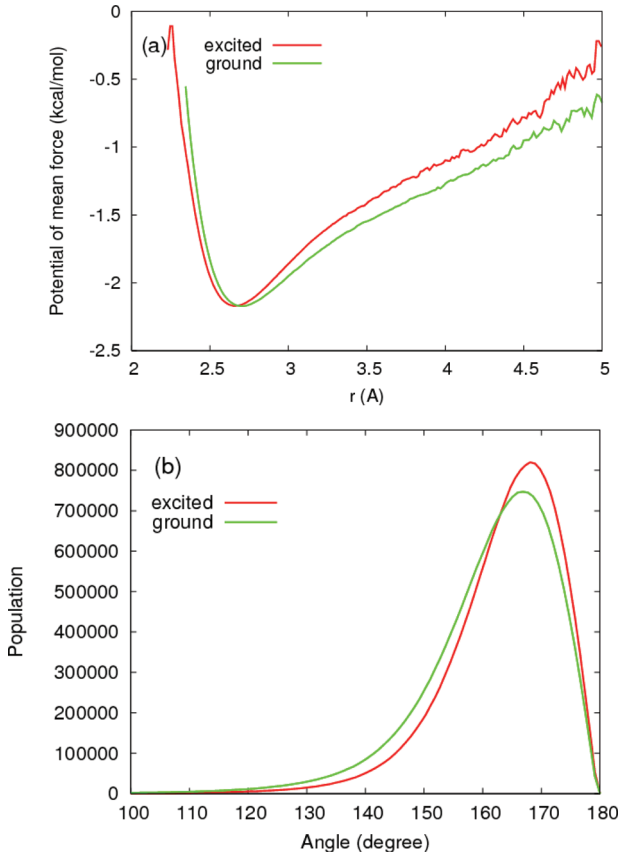

Figure 5. (a) Potential of mean force (PMF) as a function of the distance between the oxygen of the tagged OD stretch and the oxygen of the nearest neighbor MeOD, in the ground state (green) and first-excited state (red). (b) The distribution of the O–D···O angle made by the tagged OD stretch and the oxygen of its nearest neighbor MeOD, in the ground state (green) and first-excited state (red).

excited methanol molecule to form H-bonds, on the absorption and emission spectra.

Figure 6a shows the equilibrium probability density of the OD stretch transition frequency in the ground state (green) and first-excited state (red), for 10 mol % MeOD in CCl_4. Whereas the narrow high-frequency α/β peak in the excited state does not shift relative to that in the ground state, the area under the peak is smaller in the excited state. At the same time, the broad low-frequency $\gamma/\delta/\varepsilon$ peaks are seen to be red-shifted in the excited state relative to the ground state. Both trends represent spectral signatures for the higher propensity for H-bonding in the excited state. The breakdown of the equilibrium distribution of the transition frequencies, in the excited state, into its individual contributions from the α, β, γ, δ, and ε species is shown in Figure 6b (the corresponding results for the ground state was reported in ref 13).

Table 1 shows the relative populations of the different H-bonded species at 10 and 26 mol % MeOD/CCl_4 mixtures, as well as in pure MeOD, at the excited state. The numbers in parentheses correspond to the ground state populations. As expected, the subpopulations of the strongly H-bonded species (δ and ε) increase with increasing MeOD concentration at the expense of the non H-bonded (α) or weakly H-bonded (β and γ) species. Interestingly, the ε subpopulation is significant in all three concentrations and amounts to almost fifth of the hydroxyls in pure methanol. Thus, one expects pure methanol to constitute of a mixture of complex branched H-bonded

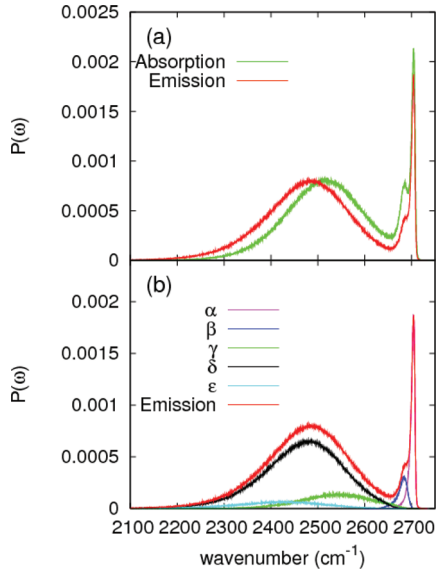

Figure 6. (a) Equilibrium probability density of the OD stretch frequency for the excited vibrational state (red) and ground state (red) in 10 mol % MeOD/CCl_4. (b) The corresponding equilibrium probability densities of the OD stretch frequency for the various H-bonded species in the excited state.

Table 1. H-Bonded Species Populations (%) of a Vibrationally Excited MeOD in 10 mol % and 26 mol % MeOD/CCl_4 Mixtures and Pure MeOD[a]

species	10 mol %	26 mol %	pure MeOD
α	10.1 (12.0)	1.6 (4.5)	0.2 (0.7)
β	3.6 (7.3)	2.1 (3.9)	0.6 (1.5)
γ	12.2 (15.7)	9.8 (11.2)	8.6 (11.1)
δ	66.5 (58.8)	72.8 (70.3)	71.3 (71.3)
ε	7.3 (5.6)	13.2 (9.3)	18.5 (14.3)

[a]The numbers in parentheses correspond to the populations in the ground vibrational state.

oligomers. Finally, one notes that the δ and ε subpopulations increase at the expense of the α, β, and γ subpopulations, when the hydroxyl is excited. This observation is consistent with the above-mentioned higher propensity for H-bonding in the excited state.

Table 2 shows the lifetimes of the different H-bonded species at the above-mentioned three different concentrations. The

Table 2. Lifetimes (in ps) of H-Bonded Species of a Vibrationally Excited MeOD in 10 mol % and 26 mol % MeOD/CCl_4 Mixtures and Pure MeOD[a]

hydrogen bond species	10 mol %	26 mol %	pure MeOD
α	1.31 (0.77)	0.32 (0.45)	0.08 (0.09)
β	0.30 (0.33)	0.20 (0.18)	0.07 (0.08)
γ	0.51 (0.49)	0.40 (0.37)	0.40 (0.38)
δ	2.46 (1.61)	2.72 (1.80)	3.04 (1.93)

[a]The numbers in parentheses correspond to the lifetimes in the ground vibrational state.

lifetime is defined as the average time it takes one species to change into another. The numbers in parentheses correspond to the lifetimes for methanol in the ground vibrational state. As expected, the lifetimes of the α and β species become shorter

dx.doi.org/10.1021/jp211792j | J. Phys. Chem. B 2012, 116, 2856–2866

with increasing concentration, while the lifetime of the γ and δ species become longer. Another notable feature is the increase of the lifetime of the γ and δ species in the excited state compared to the ground state, which is consistent with the higher propensity for H-bonding in the excited state.

Figure 7 shows the calculated OD stretch IR emission (red) and absorption (green) spectra in 10 mol % MeOD/CCl_4

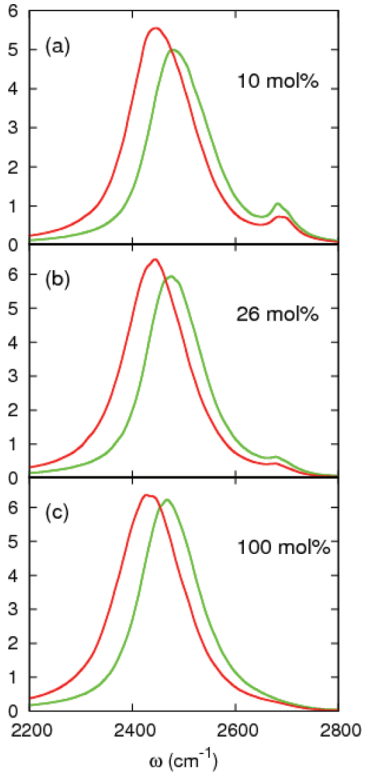

Figure 7. Calculated IR emission (red) and absorption (green) spectra of the OD stretch in 10 mol % MeOD/CCl_4 mixture (a), 26 mol % MeOD/CCl_4 mixture (b), and pure MeOD (c).

mixture (a), 26 mol % MeOD/CCl_4 mixture (b), and pure MeOD (c). The absorption and emission spectra are similar in shape. The main differences between them is that the narrow emission α/β peak is smaller than the similarly narrow absorption α/β peak, and the broad emission $\gamma/\delta/\varepsilon$ peak is larger and red-shifted relative to the similarly broad absorption $\gamma/\delta/\varepsilon$ peak. The Stokes shift, as measured by the red shift of the peak of the $\gamma/\delta/\varepsilon$ band, is give by 32.0, 31.4, and 40.3 cm^{-1} in 10 mol % MeOD/CCl_4 mixture, 26 mol % MeOD/CCl_4 mixture, and pure MeOD, respectively. As expected, the α/β peak diminishes with increasing MeOD concentration and is practically nonexistent in the case of pure methanol.

The observation that excitation of the OD stretch causes the contraction of the hydrogen bond and a red shift of the emission peak of the OD stretch is consistent with previous experimental observations and theoretical predictions for HOD/D_2O.[60−62] Woutersen and Bakker[60] have reported a Stokes shift of 70 cm^{-1} in this system, as obtained from pump−probe spectra on the OH-stretch of HOD. Lawrence and Skinner[62] have predicted a Stokes shift of 57 cm^{-1}, based on MD simulations. These values of the Stokes shift for the HOD/D_2O are slightly larger than for MeOD, as can be expected based on the $2^{-1/2}$ scaling factor due to isotope substitution from H to D and the fact that H-bonding in water is expected to be stronger than in methanol.

The interpretation of the Stokes shift as a signature of the higher propensity for H-bonding in the excited state is also consistent with the observation that the absorption and emission spectra are seen to coincide at infinite dilution (i.e., with a single MeOD and 255 CCl_4 molecules in the simulation box), where H-bonding is absent (not shown). This implies that solvation by CCl_4 does not give rise to a noticeable Stokes shift and that the Stokes shift between emission and absorption can be solely attributed to H-bonding interactions. Interestingly, the fwhm for α is significantly broader than the experimental value of 20 cm^{-1}.[22−24] This discrepancy suggests that the MeOD-CCl_4 interaction as described by the force fields used is too strong. In contrast, the fact that the fwhm of the γ species is comparable to the experimental value of ∼80 cm^{-1},[24] can be attributed to the fact that the MeOD−MeOD interactions are captured accurately by the force fields.

C. Nonlinear Mapping Relations. The mixed quantum-classical procedure outlined in section II is computationally costly due to the need for on-the-fly diagonalization. However, as we have shown in ref 13, the computational cost can be reduced to that of a classical MD simulation if one can establish nonlinear mapping relations between the transition frequency and OD bond length (defined as the expectation value of the bond length of the tagged hydroxyl) and the electric field along the hydroxyl bond. Such relations were presented in ref 13 in the case when the tagged OD stretch is in the ground state. Here, we extend the analysis by establishing similar nonlinear mapping relations for the case when the tagged OD stretch is in the first-exited state.

A scatter plot of the OD stretch transition frequency as a function of the magnitude of the electric field along the OD bond when the OD stretch is in the ground state (green) and excited state (red) is shown in Figure 8a. As can be seen there is a strong correlation between these two quantities which can be used in order to generate mapping relations between them. Such mapping relations can be obtained by a least-squares fit to a polynomial function (see Figure 8a). The mapping relations that correlate the transition frequency with the electric field is seen to be rather insensitive to the quantum state of the OD stretch. The polynomial expression for the ground state mapping relation was given in ref 13. The polynomial expression for the excited state mapping relation is given by (the frequency ω is in cm^{-1} and the electric field x is given in units of e/a_0^2)

$$\begin{aligned}\omega(x) = {} & 2698.60 - 2808.46x + 58360.6x^2 \\ & - 2.85703 \times 10^7 x^3 + 1.76775 \times 10^9 x^4 \\ & - 5.06397 \times 10^{10} x^5 + 7.48760 \times 10^{11} x^6 \\ & - 5.56162 \times 10^{12} x^7 + 1.63910 \times 10^{13} x^8 \end{aligned} \quad (18)$$

Figure 8b shows the correlation between the OD bond length and the electric field along the OD bond. Here too, one observes a strong correlation between these two quantities. It should be noted that a similar correlation was found in the ground state.[13] In fact, the correlation is very similar in both cases except for the fact that the OD bond length in the excited state is shifted to higher values than in the ground state, which can be traced back to the higher propensity for H-bonding in the excited state. The polynomial expression for the corresponding ground state mapping relation was given in ref 13.

dx.doi.org/10.1021/jp211792j | J. Phys. Chem. B 2012, 116, 2856−2866

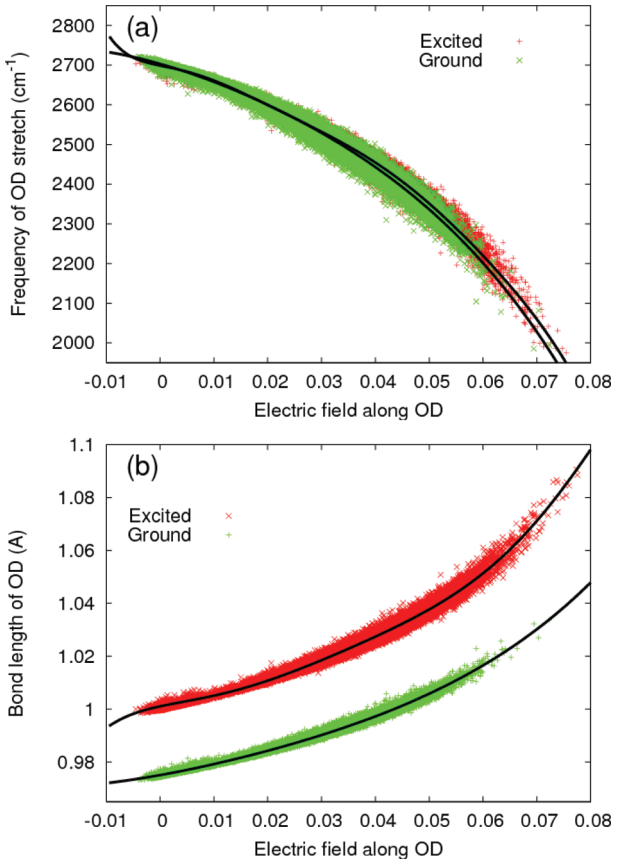

Figure 8. Scatter plot of the ground state (green) and vibrationally excited (red) OD stretch frequency (a) and OD bond length (b) as a function of the electric field along the OD bond axis, as obtained from a mixed quantum-classical simulation in 10 mol % MeOD/CCl_4 mixture. The solid lines are the polynomial fit to the scatter plots.

The polynomial expression for the excited state mapping relation is given by (the OD stretch bond length is in Å and the electric field x is given in units of e/a_0^2)

$$r_{OD}(x) = 1.00105 + 0.44395x - 16.2237x^2 + 1621.62x^3 - 45384.3x^4 + 552688x^5 - 2.35394x^6 \quad (19)$$

Classical MD simulations can therefore be performed, where the OD stretch frequency at each time step is obtained from eq 18, instead of via solving the Schrödinger equation on-the-fly, and the tagged OD bond length is modified based on eq 19. Figure 9 shows a comparison of the emission line shape obtained via this procedure for 10 mol % MeOD system in comparison to the mixed quantum-classical procedure that involves costly on-the-fly diagonalization. The agreement between the two emission spectra is excellent.

Also shown in Figure 9 is the result of a classical simulation using only eq 18 with the fixed OD bond of 0.96 Å which is the AMBER force field value of the bond length. This result is clearly not in good agreement with the mixed quantum-classical result. Thus, in order to reproduce the mixed quantum-classical MD simulation result, one should take into account the change of the OD bond length in addition to the OD frequency.

D. Excited State Lifetime for the OD Stretch Mode. As indicated in section II.E, the relaxation from the excited state to the ground state can be treated as a nonadiabatic process. The nonadiabatic coupling vector **d**, eq 16, is a 3N-dimensional

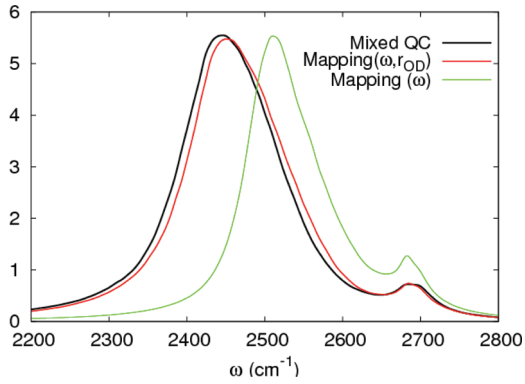

Figure 9. IR emission lineshapes in 10 mol % MeOD/CCl_4, calculated from: (1) A mixed quantum-classical simulation (black); (2) a classical simulation with the mapping relations between the OD transition frequency and bond length, and the electric field along the OD bond axis (red); (3) a classical simulation with only the mapping relation between the OD transition frequency and the electric field along the OD bond axis (green).

vector where N is the number of atoms. Further insight into its behavior can be obtained by considering the following correlation functions $\langle \mathbf{d}(0)\cdot\mathbf{d}(t)\rangle$, $\langle \hat{\mathbf{d}}(0)\cdot\hat{\mathbf{d}}(t)\rangle$, and $\langle d(0)\cdot d(t)\rangle$, where $\hat{\mathbf{d}} = \mathbf{d}/d$ and $d = (\mathbf{d}\cdot\mathbf{d})^{1/2}$ are the unit vector along **d** and its length, respectively (see Figure 10). The

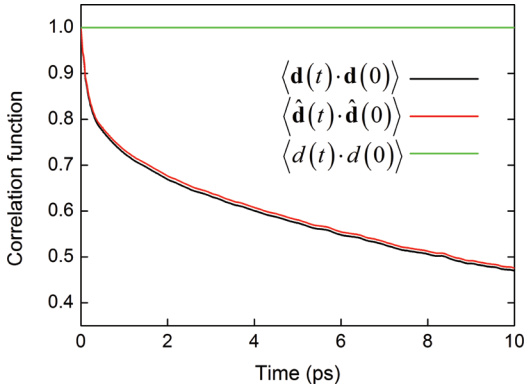

Figure 10. The normalized correlation functions $\langle \mathbf{d}(0)\cdot\mathbf{d}(t)\rangle$, $\langle \hat{\mathbf{d}}(0)\cdot\hat{\mathbf{d}}(t)\rangle$, and $\langle d(0)\cdot d(t)\rangle$, where $\hat{\mathbf{d}} = \mathbf{d}/d$ and $d = (\mathbf{d}\cdot\mathbf{d})^{1/2}$ are the unit vector along **d** and its length, respectively (calculated for 10 mol % MeOD/CCl_4 mixture).

main observation from Figure 10 is that the decay of $\langle \mathbf{d}(0)\cdot\mathbf{d}(t)\rangle$ is caused by rotational relaxation of this vector. In what follows, we therefore assume that the length of this vector is fixed and given by its excited state equilibrium average value, and determine its instantaneous orientation via the procedure outlined below.

We start out by defining

$$\mathbf{f}(\mathbf{Q}, q) = -\nabla_{\mathbf{R}} V_1(\mathbf{Q}, q) \quad (20)$$

In the next step we take advantage of the fact that the amplitude of the fluctuations of q relative to its equilibrium value, q_0, are small, in order to approximate $\mathbf{f}(\mathbf{Q},q)$ by its first-order expansion in q around q_0

$$\mathbf{f}(\mathbf{Q}, q) \approx \mathbf{f}(q_0) + \mathbf{G}(q - q_0) \quad (21)$$

dx.doi.org/10.1021/jp211792j | J. Phys. Chem. B 2012, 116, 2856–2866

where $\mathbf{G} = (\Delta\mathbf{f}/\Delta q)|_{q=q_0}$. The numerator in the second equality in eq 16 can therefore be given by

$$\langle\psi_0|\mathbf{f}(q)|\psi_1\rangle \approx \langle\psi_0|\mathbf{f}(q_0)|\psi_1\rangle + \mathbf{G}\langle\psi_0|q|\psi_1\rangle = \mathbf{G}\langle\psi_0|q|\psi_1\rangle \quad (22)$$

Equation 22 therefore implies that $\mathbf{d}$ and $\mathbf{G}$ are parallel, so that the direction of the former can be obtained from that of the latter. Thus the quantity $\mathbf{d}(\mathbf{R}_t)\cdot\dot{\mathbf{R}}_t$ can be calculated as

$$\mathbf{d}(\mathbf{R}_t)\cdot\dot{\mathbf{R}}_t = (\hat{\mathbf{d}}(\mathbf{R}_t)\cdot\dot{\mathbf{R}}_t)d \approx (\hat{\mathbf{G}}(\mathbf{R}_t)\cdot\dot{\mathbf{R}}_t)d \quad (23)$$

In Figure 11 we demonstrate the validity of this approximation by comparing these two quantities, $\hat{\mathbf{d}}(\mathbf{R}_t)\cdot\dot{\mathbf{R}}_t$ and $\hat{\mathbf{G}}(\mathbf{R}_t)\cdot(\dot{\mathbf{R}}_t)$,

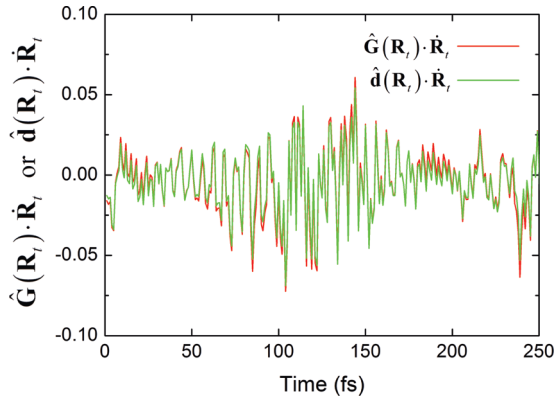

Figure 11. Comparison of $\hat{\mathbf{d}}(t)\cdot\dot{\mathbf{R}}(t)$ and $\hat{\mathbf{G}}(t)\cdot\dot{\mathbf{R}}(t)$ for 10 mol % MeOD/CCl_4 mixture.

along a 250 fs long trajectory in the case of 10 mol % MeOD/CCl_4. Figure 11 proves that the vector $\mathbf{G}$ can be assumed to be parallel to the vector $\mathbf{d}$.

Figure 12 shows $k_{01}(\omega)$ as a function of ω, on a semilog plot, as calculated for 10 mol % MeOD in CCl_4. The vertical line

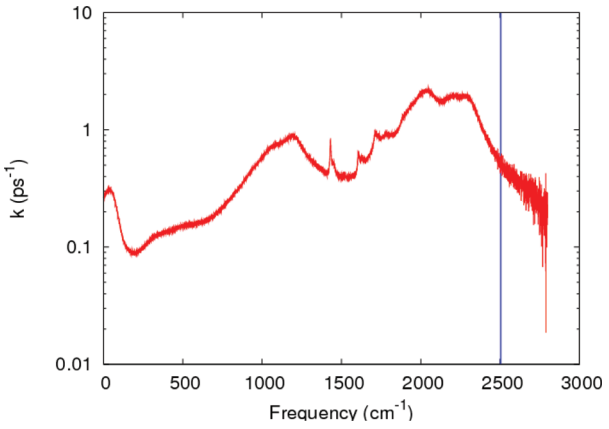

Figure 12. $k_{01}(\omega)$ as a function of ω, on a semilog plot, as calculated for 10 mol % MeOD in CCl_4. The vertical line indicates the average value of ω that corresponds to the average excited state transition frequency for the OD stretch in this system, $\langle\omega_{10}\rangle_1 = 2504$ cm^{-1}.

indicates the average value of ω that corresponds to the average excited state transition frequency for the OD stretch in this system, $\langle\omega_{10}\rangle_1 = 2504$ cm^{-1}. The actual value of the lifetime is 1.95 ± 0.09 ps (see Table 3). The experimental lifetime is 0.66 ps, which is defined as the time it takes $\sum_j P_j \exp[-t/T_1^j]$ to decay to e^{-1} of its initial value, where $j = \alpha/\beta, \gamma, \delta$, P_j is the calculated population of a species and T_1^j is its experimental lifetime (see Table 3). Although the calculated lifetime is about three times slower than the experimental lifetime, we consider this level of agreement as reasonable if one takes into account the somewhat ad-hoc nature of the quantum correction factor used and uncertainties regarding the force fields.

Table 3. Excited State Lifetimes

species	experimental lifetime (ps)	relative populations from simulation (%)	average experimental lifetime (ps)	average calculated lifetime (ps)
α/β	2.15	13.7		
γ	1.0	12.2	0.66	1.95 ± 0.09
δ	0.5	66.5		

The large peaks above 1000 and 2000 cm^{-1} suggest a possibility that vibrational population relaxation occurs via energy transfer to other intramolecular vibrational modes. In this context, it is interesting to point out that Rey and Hynes,[64] and later Lawrence and Skinner[65] have argued that vibrational relaxation of the OH stretch in HOD/D_2O occurs via energy transfer from the OH stretch to the bending overtone of HOD. The experimentally observed frequency of the CO stretch mode for the methanol molecule is about 1040 cm^{-1} and that of the COD bending is 864 cm^{-1}.[66] Thus, energy transfer to the overtone or fundamental transitions of the CO stretch or COD bending is a likely mechanism for the relaxation of the excited OD stretch. However, a detailed investigation of the mechanism is beyond the scope of this paper, and will be reserved for future work.

The magnitude of the harmonic-Schofield quantum correction factor evaluated by eq 17 with $\langle\omega_{10}\rangle_1 = 2504$ cm^{-1} is 69.7. Several other choices for the quantum correction factor were discussed and compared in ref 56. The standard, harmonic, and Scofield quantum correction factors, as evaluated with $\langle\omega_{10}\rangle_1 = 2504$ cm^{-1}, are given by 2, 12, and 405, respectively. Closely related to the present work are the series of works done by Staib.[5,10,11] Staib[11] used the so-called standard quantum correction factor for calculating the lifetimes of the first excited state of the OH stretch in the case of a methanol monomer and dimer in CCl_4, and obtained lifetimes of 850 ns for monomer and 12 ns for dimer, which are significantly larger than the result of the present work.

Table 4 shows the lifetimes at six different frequencies for 10 mol %, 26 mol %, and pure MeOD cases. These values are compared to the experimental values reported in ref 24 for 0.8 mol % methanol-*d*/23 mol % methanol-*h* dissolved in CCl_4. Although the calculated lifetimes are all larger than the experimental ones, the trend of increasing lifetime with increasing frequency is reproduced reasonably well.

Since the extent of H-bonding associated with the species decreases with increasing frequency, this trend implies that the extra interactions brought about by H-bonding facilitate the relaxation of the OD stretch from the excited to the ground state. This also explains the fact that the lifetime becomes shorter with increasing MeOD concentration, since a higher MeOD concentration implies more H-bonding (see Table 4).

IV. CONCLUDING REMARKS

In a previous paper,[13] we showed how combining our mixed quantum-classical methodology with the appropriate choice of force fields, one can reproduce the experimental absorption IR spectrum of the hydroxyl stretch in methanol/CCl_4 liquid

dx.doi.org/10.1021/jp211792j | J. Phys. Chem. B 2012, 116, 2856–2866

Table 4. Excited State Lifetimes, As a Function of Frequency, of a Vibrationally Excited MeOD in 10 mol % and 26 mol % MeOD/CCl_4 Mixtures and Pure MeOD

	2450 cm^{-1}	2470 cm^{-1}	2490 cm^{-1}	2510 cm^{-1}	2530 cm^{-1}	2550 cm^{-1}
10 mol % MeOD/CCl_4	1.44 ± 0.06	1.63 ± 0.07	1.82 ± 0.08	2.00 ± 0.09	2.17 ± 0.11	2.31 ± 0.12
26 mol % MeOD/CCl_4	1.29 ± 0.02	1.43 ± 0.02	1.56 ± 0.02	1.68 ± 0.02	1.80 ± 0.03	1.91 ± 0.03
pure MeOD	1.09 ± 0.003	1.20 ± 0.003	1.30 ± 0.01	1.40 ± 0.01	1.48 ± 0.01	1.56 ± 0.01
experiment	0.42	0.43	0.46	0.53	0.70	0.90

mixtures rather accurately, for different isotopomers and on a wide range of compositions. We have also been able to utilize this approach in order to shed light on the relationship between different features in the absorption spectrum and the underlying ground state H-bonding structure and dynamics.

In order to achieve this level of consistency without adjustable parameters, we found it necessary to account for the anharmonic nature of the tagged hydroxyl stretch and polarizable nature of the force fields, as well as the damping of the polarizability at short distances. We have also shown that one can utilize nonlinear mapping relations between the hydroxyl transition frequency and bond length and the electric field along the hydroxyl bond axis in order to reduce the computational cost of the mixed quantum-classical treatment to that of a purely classical MD simulation.

In the present paper, we showed that the agreement with the experimental IR absorption spectrum can be further improved by accounting for the dependence of μ' on the solvent configuration. We have also extended the analysis to H-bonding structure and dynamics of the vibrationally excited hydroxyl and explored their signature on the IR emission spectrum and excited state lifetime. Our new results regarding the excited state are also seen to be consistent with experimental data when available, thereby providing further support for the accuracy of the model and its ability to shed new light on the molecular structure and dynamics of this rather complex condensed phase system.

We have found that the vibrationally excited hydroxyl has a higher propensity for H-bonding in comparison to the hydroxyl in the vibrational ground state. We have also found that the difference in H-bonding between the ground and excited states is responsible for the sizable (~30−40 cm^{-1} for MeOD) red Stokes shift between the emission and absorption $\gamma/\delta/\varepsilon$ bands. Treating the relaxation from the excited state to the ground state as a nonadiabatic process, and calculating its rate within the framework of Fermi's golden rule and the harmonic-Schofield quantum correction factor, we were able to obtain a lifetime which is slower by a factor of 3 from the experimental value, which we consider to be relatively reasonable agreement. In addition we were able to reproduce the experimentally observed dependence of the lifetime on the transition frequency rather accurately.

it should be noted that H-bonded alcohol oligomers are also believed to exhibit interesting photochemistry upon relaxation from the excited state to the ground state. More specifically, since the energy released upon the relaxation of the photoexcited hydroxyl stretch back to the ground state can result in breaking of H-bonds in its vicinity, which is believed to have a pronounced signature on pump−probe IR spectra.[22−30,36] Work on extending the mixed quantum-classical methodology presented herein to account for these processes is currently underway and will be reported in a future publication.

AUTHOR INFORMATION

Corresponding Author

*E-mail: kjkwac@umich.edu; eitan@umich.edu.

Notes

The authors declare no competing financial interest.

ACKNOWLEDGMENTS

This project was supported by the National Science Foundation through Grant CHE-1111495.

REFERENCES

(1) Jorgensen, W. L. *J. Am. Chem. Soc.* **1980**, *102*, 543−549.
(2) Palinkas, G.; Hawlicka, E.; Heinzinger, K. *J. Phys. Chem.* **1987**, *91*, 4334−4341.
(3) Haughney, M.; Ferrario, M.; McDonald, I. R. *J. Phys. Chem.* **1987**, *91*, 4934−4940.
(4) Matsumoto, M.; Gubbins, K. E. *J. Chem. Phys.* **1990**, *93*, 1981−1994.
(5) Meyer zum Büschenfelde, D.; Staib, A. *Chem. Phys.* **1998**, *236*, 253−261.
(6) Curtiss, L. A. *J. Chem. Phys.* **1977**, *67*, 1144−1149.
(7) Mo, O.; Yanez, M.; Elguero, J. *THEOCHEM J. Mol. Struct.* **1994**, *120*, 73−81.
(8) Dixon, J. R.; George, W. O.; Hossain, M. F.; Lewis, R.; Price, J. M. *J. Chem. Soc. Faraday Trans.* **1997**, *93*, 3611−3618.
(9) Ohno, K.; Shimoaka, T.; Akai, N.; Katsumoto, Y. *J. Phys. Chem. A* **2008**, *112*, 7342−7348.
(10) Staib, A.; Borgis, D. *Chem. Phys. Lett.* **1997**, *271*, 232−240.
(11) Staib, A. *J. Chem. Phys.* **1998**, *108*, 4554−4562.
(12) Veldhuizen, R.; de Leeuw, S. W. *J. Chem. Phys.* **1996**, *105*, 2828−2836.
(13) Kwac, K.; Geva, E. *J. Phys. Chem. B* **2011**, *115*, 9184−9194.
(14) Errera, J.; Mollet, P. *Nature* **1936**, *138*, 882.
(15) Liddel, U.; Becker, E. D. *Spectrochim. Acta Part A* **1957**, *10*, 70−84.
(16) Bellamy, L. J.; Pace, R. J. *Spectrochim. Acta* **1966**, *22*, 525−533.
(17) Bonner, O. D. *J. Chem. Thermodyn.* **1970**, *2*, 577−581.
(18) Graener, H.; Ye, T. Q.; Laubereau, A. *J. Chem. Phys.* **1989**, *91*, 1043−1046.
(19) Laenen, R.; Rauscher, C. *J. Chem. Phys.* **1997**, *106*, 8974−8980.
(20) Bertie, J. E.; Zhang, S. L. *J. Mol. Struct.* **1997**, *413*−*414*, 333−363.
(21) Kristiansson, O. *J. Mol. Struct.* **1999**, *477*, 105−111.
(22) Levinger, N. E.; Davis, P. H.; Fayer, M. D. *J. Chem. Phys.* **2001**, *115*, 9352−9360.
(23) Gaffney, K. J.; Piletic, I. R.; Fayer, M. D. *J. Phys. Chem. A* **2002**, *106*, 9428−9435.
(24) Gaffney, K. J.; Davis, P. H.; Piletic, I. R.; Levinger, N. E.; Fayer, M. D. *J. Phys. Chem. A* **2002**, *106*, 12012−12023.
(25) Asbury, J. B.; Steinel, T.; Stromberg, C.; Gaffney, K. J.; Piletic, I. R.; Goun, A.; Fayer, M. D. *Phys. Rev. Lett.* **2003**, *91*, 23742.
(26) Asbury, J. B.; Steinel, T.; Stromberg, C.; Gaffney, K. J.; Piletic, I. R.; Fayer, M. D. *J. Chem. Phys.* **2003**, *119*, 12981−12997.
(27) Asbury, J. B.; Steinel, T.; Stromberg, C.; Gaffney, K. J.; Piletic, I. R.; Goun, A.; Fayer, M. D. *Chem. Phys. Lett.* **2003**, *374*, 362−371.
(28) Asbury, J. B.; Steinel, T.; Fayer, M. D. *J. Phys. Chem. B* **2004**, *108*, 6544−6554.

(29) Asbury, J. B.; Steinel, T.; Stromberg, C.; Corcelli, S. A.; Lawrence, C. P.; Skinner, J. L.; Fayer, M. D. *J. Phys. Chem. A* **2004**, *108*, 1107−1119.
(30) Asbury, J. B.; Steinel, T.; Fayer, M. D. *J. Lumin.* **2004**, *107*, 271−286.
(31) Gulmen, T. S.; Sibert, E. L. III. *J. Phys. Chem. A* **2005**, *109*, 5777−5780.
(32) Gulmen, T. S.; Sibert, E. L. III. *J. Chem. Phys.* **2005**, *123*, 204508.
(33) Iwaki, L. K.; Dlott, D. D. *J. Phys. Chem. A* **2000**, *104*, 9101−9112.
(34) Iwaki, L. K.; Dlott, D. D. *Chem. Phys. Lett.* **2000**, *321*, 419−425.
(35) Wang, Z.; Pakoulev, A.; Dlott, D. D. *Science* **2002**, *296*, 2201−2203.
(36) Graener, H.; Ye, T. Q.; Laubereau, A. *J. Chem. Phys.* **1989**, *90*, 3413−3416.
(37) Heilweil, E. J.; Casassa, M. P.; Cavanagh, R. R.; Stephenson, J. C. *J. Chem. Phys.* **1986**, *85*, 5004−5018.
(38) Laenen, R.; Gale, G. M.; Lascoux, N. *J. Phys. Chem. A* **1999**, *103*, 10708−10712.
(39) Laenen, R.; Simeonidis, K. *Chem. Phys. Lett.* **1999**, *299*, 589−596.
(40) Woutersen, S.; Emmerichs, U.; Bakker, H. J. *J. Chem. Phys.* **1997**, *107*, 1483−1490.
(41) Case, D.; Darden, T.; Cheatham, T.; I. I. I.; Simmerling, C.; Wang, J.; Duke, R.; Luo, R.; Crowley, M.; Walker, R.; Zhang, W. et al. *AMBER 10*; University of California: San Francisco, CA, 2008.
(42) Duffy, E. M.; Severance, D. L.; Jorgensen, W. L. *J. Am. Chem. Soc.* **1992**, *114*, 7535−7542.
(43) Applequist, J.; Carl, J. R.; Fung, K. K. *J. Am. Chem. Soc.* **1972**, *94*, 2952.
(44) Caldwell, J. W.; Kollman, P. A. *J. Phys. Chem.* **1995**, *99*, 6208−6219.
(45) Alfredsson, M.; Brodholt, J. P.; Hermanson, K.; Vallauri, R. *Mol. Phys.* **1998**, *94*, 873−876.
(46) Masia, M.; Probst, M.; Rey, R. *J. Chem. Phys.* **2005**, *123*, 164505.
(47) Thole, B. T. *Chem. Phys.* **1981**, *59*, 341−350.
(48) Cieplak, P.; Dupradeau, F.-Y.; Duan, Y.; Wang, J. *J. Phys.:Condens. Matter* **2009**, *21*, 333102.
(49) Bernardo, D. N.; Ding, Y.; Krogh-Jespersen, K.; Levy, R. M. *J. Phys. Chem.* **1994**, *98*, 4180−4187.
(50) Berendsen, H. J. C.; Postma, J. P. M; van Gunsteren, W. F.; DiNola, A.; Haak, J. R. *J. Chem. Phys.* **1984**, *81*, 3684−3690.
(51) Mukamel, S. *Principles of Nonlinear Optical Spectroscopy*; Oxford: New York, 1995.
(52) Corcelli, S. A.; Skinner, J. L. *J. Phys. Chem. A* **2005**, *109*, 6154−6165.
(53) Dapprich, S.; Komaromi, I.; Byun, K. S.; Morokuma, K.; Frisch, M. J. *J. Mol. Struct. THEOCHEM* **1999**, *462*, 1−21.
(54) Frisch, M. J.; Trucks, G. W.; Schlegel, H. B.; Scuseria, G. E.; Robb, M. A.; Cheeseman, J. R.; Scalmani, G.; Barone, V.; Mennucci, B.; Petersson, G. A. et al. *Gaussian 09*; Gaussian Inc.: Wallingford, CT, 2009.
(55) Hanna, G.; Kapral, R. *J. Chem. Phys.* **2005**, *122*, 244505.
(56) Egorov, S. A.; Everitt, K. F.; Skinner, J. L. *J. Phys. Chem. A* **1999**, *103*, 9494.
(57) Skinner, J. L.; Park, K. *J. Phys. Chem. B* **2001**, *105*, 6716.
(58) Everitt, K. F.; Skinner, J. L.; Ladanyi, B. M. *J. Chem. Phys.* **2002**, *116*, 179−183.
(59) Shi, Q.; Geva, E. *J. Phys. Chem. A* **2004**, *108*, 6109.
(60) Woutersen, S.; Bakker, H. J. *Phys. Rev. Lett.* **1999**, *83*, 2077.
(61) Wang, Z.; Pang, Y.; Dlott, D. D. *J. Chem. Phys.* **2004**, *120*, 8345.
(62) Lawrence, C. P.; Skinner, J. L. *J. Chem. Phys.* **2002**, *117*, 8847.
(63) Schmidt, J. R.; Corcelli, S. A.; Skinner, J. L. *J. Chem. Phys.* **2005**, *123*, 044513.
(64) Rey, R; Hynes, J. T. *J. Chem. Phys.* **1996**, *104*, 2356.
(65) Lawrence, C. P.; Skinner, J. L. *J. Chem. Phys.* **2002**, *117*, 5827.
(66) Serrallach, A.; Meyer, R.; Günthard, Hs. H. *J. Mol. Spectrosc.* **1974**, *52*, 94.